# Tritiated Amorphous Silicon Betavoltaic Devices

Introduction

Hydrogenated amorphous silicon (a-Si:H) is an amorphous semiconductor whose optoelectronic properties, combined with its relatively low cost of fabrication, have made it an established material in semiconductor technology, particularly for photovoltaics and active matrix displays.[1,2]

When prepared by conventional evaporation or sputtering, thin films of amorphous silicon contain a large concentration of defects and microvoids.[3,4] These give rise to localized states in the energy gap of the material.[3,4] Plasma-enhanced chemical vapor deposition (PECVD), using silicon hydrides, significantly reduces the number of defects and thereby lowers the concentration of localized states in the energy gap.[3–5] It is well known that hydrogen is responsible for defect passivation.[3–5] Hydrogen atoms incorporated into these films satisfy the covalent bonds at defects and microvoids and also allow the lattice to relax, thereby reducing the density of localized states by several orders of magnitude.[3–5]

Tritium (T) is an isotope of hydrogen and is expected to readily replace hydrogen in a-Si:H.[6] Tritium is radioactive and undergoes beta decay according to the following reaction:

$$^3\text{H} \rightarrow {}^3\text{He}^+ + \beta^- + \bar{\nu}, \qquad (1)$$
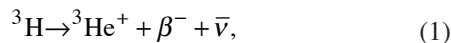
where β^- is a beta particle and $\bar{\nu}$ is an antineutrino. The antineutrino is essentially undetectable; thus tritium is considered to be a pure beta emitter. The half-life of tritium is 12.3 years, or equivalently the decay rate of tritium is $1.78 \times 10^{-9}\,\text{s}^{-1}$. Accordingly, 1 cm^3 of tritium at standard temperature and pressure has an activity of 2.6 Ci. The kinetic energy spectrum of beta particles produced from the decay of tritium is shown in Fig. 95.52.[7] The maximum energy of the beta particles is 18.6 keV while the average energy is 5.7 keV. Considering the energy distribution, the power available from the kinetic energy of the beta particles is 33.7 μW/Ci.

In theory, for 1 at. % of tritium in silicon, the power released in a 1-μm film of tritiated amorphous silicon (a-Si:H:T) will be 0.08 μW/cm^2. The average range of a 5.7-keV beta particle in silicon is 0.17 μm; thus most of this power is trapped in the film. The incorporation of tritium into a-Si:H is expected to give rise to a family of devices in which the energy output of the radioactive process of tritium decay is integrated with the optoelectronic properties of a-Si:H.
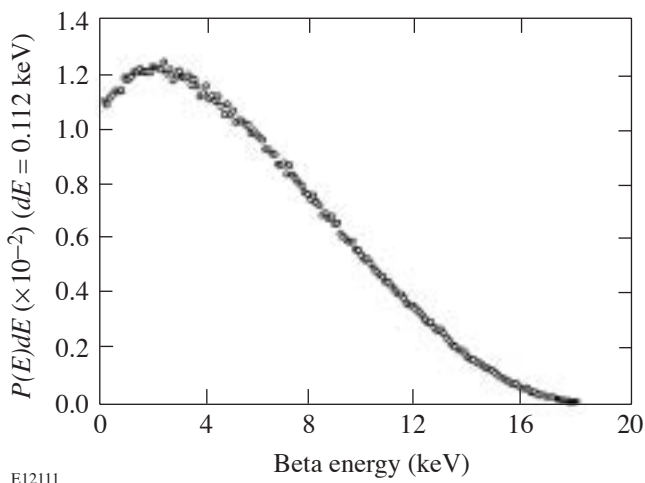

E12111

Figure 95.52
Kinetic energy spectrum of beta particles produced from the decay of tritium.[7]

Deposition of Tritiated Amorphous Silicon

A schematic of the saddle-field glow-discharge facility for the preparation of tritiated amorphous silicon is shown in Fig. 95.53. The deposition chamber is outfitted with three coarse stainless steel mesh electrodes, as shown. A glow discharge is created between the central electrode (the anode) and the outer two electrodes (the cathodes). A heated, electrically isolated substrate holder is mounted in the chamber. The substrate holder can be electrically biased.

Silane, diborane, and phosphine are available through a common port on the chamber. Tritium, which is stored as a tritide on a depleted uranium bed, is available through another port on the chamber. Each gas source is equipped with a mass-flow controller to permit independent control of flow. Evacu-ation of the deposition facility is provided by an oil-free system, which consists of a molecular drag pump and a diaphragm pump. A scrubber system, positioned between the two vacuum pumps, is used to strip tritium from the chamber effluent. The deposition system is housed in a nitrogen-atmo-sphere glovebox.

The four deposition conditions used to grow the samples that are discussed in this article are listed in Table 95.III.
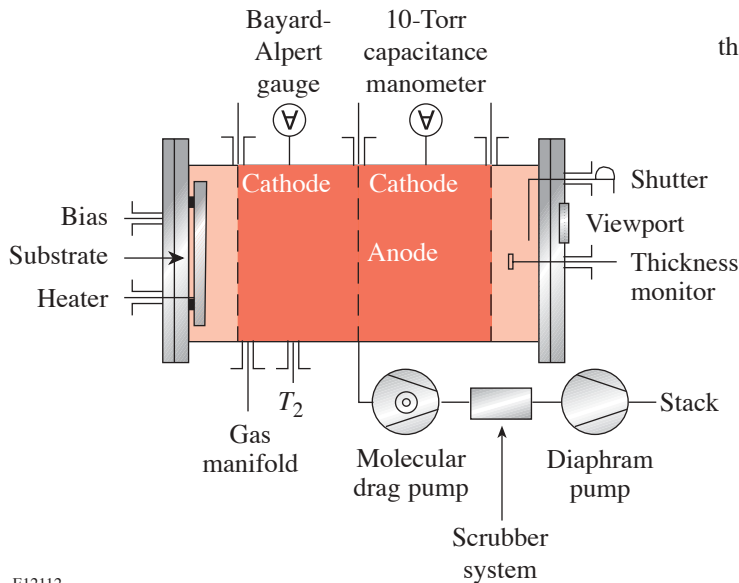

Figure 95.53
Saddle-field glow-discharge apparatus for the preparation of tritiated amorphous semiconductors.
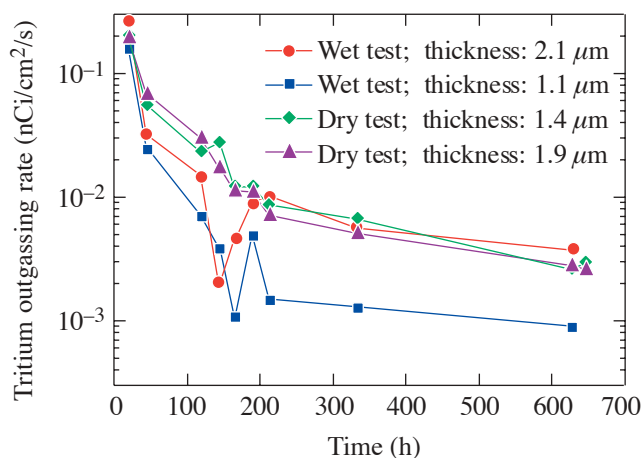
E12112

Table 95.III: Deposition conditions of the samples described in this article.

	Deposition A	Deposition B	Deposition C	Deposition D
Gas flow	2.5 sccm SiH_4	2.5 sccm SiH_4	2.5 sccm SiH_4	2.5 sccm SiH_4
	2.5 sccm T_2	2.5 sccm T_2	2.5 sccm T_2	2.5 sccm T_2
Pressure	50 mTorr	50 mTorr	50 mTorr	50 mTorr
Anode potential	700 to 710 V	610 to 650 V	580 to 620 V	1010 to 1120 V[a]
				590 to 600 V[b]
Anode current	4 mA	4 mA	30 mA	22 to 24 mA[a]
				30 mA[b]
Substrate potential	Ground	Ground	Ground	Floating 350 V[a], 280 V[b]
Substrate current	0.4 mA	0.4 mA	7 to 8 mA	—
Substrate temperature	300°C	225°C	150°C	150°C
Samples described in this article	N/A	A69	A155, A170, G181	A206, A212, A214

[a]During the first half of deposition.
[b]During the second half of deposition.

Tritium Outgassing

The rate of tritium outgassing, at room temperature, from as-deposited tritiated amorphous silicon films [5 to 10 at. % of tritium, as measured by infrared spectroscopy (see Fig. 95.57)] was estimated by measuring the evolution of tritiated water from a number of a-Si:H:T samples under dry and wet or humid air ambient, as described in Ref. 8. Experimental results show that after approximately 600 h of outgassing, the total quantity of tritium desorbed from each of the samples is less than 40 μCi/cm^2. The cumulative tritium desorption under dry and wet conditions is of the same order of magnitude. This suggests that to first order, HTO is the predominant desorbing species. The rate of tritium outgassing for four samples at room temperature is shown in Fig. 95.54. The rate of outgassing is comparable for samples in dry and wet atmospheres. The a-Si:H:T samples show an initial outgassing rate of the order of 200 pCi/cm^2/s^1. After about 600 h of outgassing, the tritium outgassing rate appears to approach a value of less than 10 pCi/cm^2/s^1 or less than one part in 10^9 s^{-1} from a 1-μm film with 5 at. % of tritium. This suggests that the top few monolayers of the film are the source of the outgassing tritium.
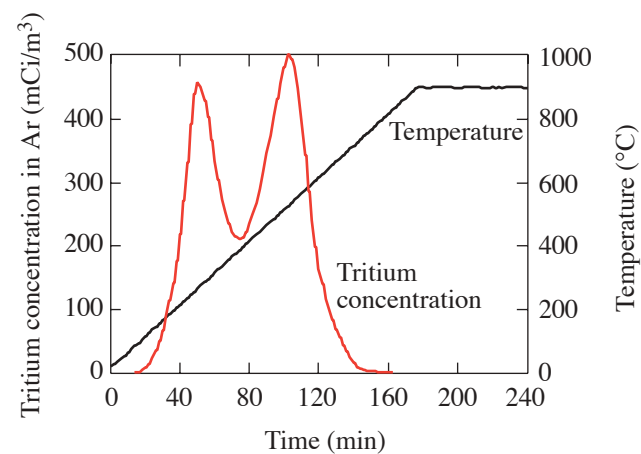

E12113

Figure 95.54
Outgassing rate from four a-Si:H:T films from deposition D (see Table 95.III).

Effusion of Tritium

Samples of a-Si:H:T were subjected to linear temperature ramping from room temperature to approximately 900°C in an argon purge. The experimental setup for tritium effusion measurements is described elsewhere.[9] The effusion experiments were carried out at temperature ramp rates of 5, 10, 20, and 40°C/min. The tritium evolution data for two samples grown at two different substrate temperatures are shown in Figs. 95.55 and 95.56. The thickness of the samples was ~0.8 μm for

sample A155 (Fig. 95.55) and ~0.2 μm for sample A69 (Fig. 95.56). The *x* axis indicates time while the *y* axis on the left shows the tritium concentration. The *y* axis on the right indicates the temperature of the sample.

It can be seen that significant tritium evolution occurs only when the sample temperature exceeds the growth temperature. At temperatures below the growth temperature but above room temperature there is an increase in the tritium monitor signal that is equivalent to a tritium concentration change of 100 μCi/m^3 in a volume of 1 L. This evolution is mainly due to surface tritium and represents a surface tritium concentra-

E12114

Figure 95.55
Tritium evolution from an a-Si:H:T film (A155) grown at 150°C.
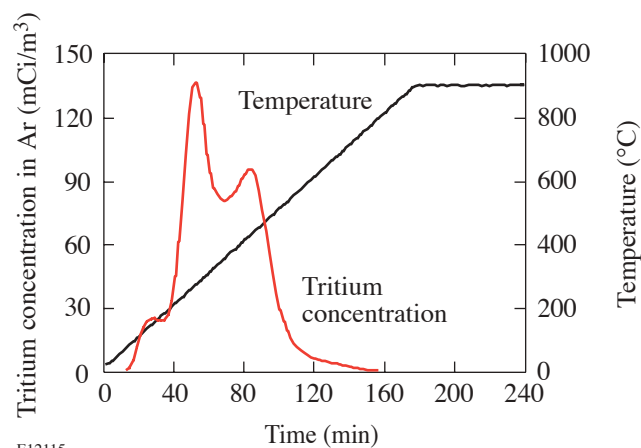
E12115

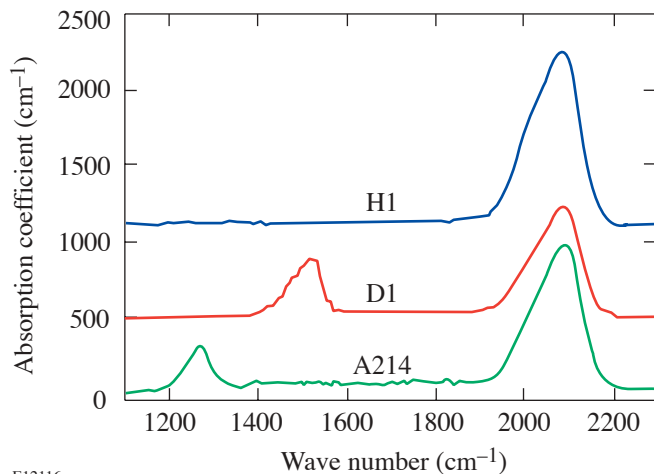Figure 95.56
Tritium evolution from an a-Si:H:T film (A69) grown at 225°C.

tion of about 10 μCi/cm^2; this is of the same order of magnitude as that measured in the outgassing experiments presented above (40 μCi/cm^2). Alternatively, the total number of hydrogen atoms on the surface can be estimated to be 6×10^{14} cm^{-2}. To put this number in context, the number of silicon atoms constituting a monolayer is about 10^{15} cm^{-2}. Considering that the total atomic hydrogen content in these films is around 15 to 30 at. %, the foregoing numbers suggest that the surface hydrogen originates from the top two to three monolayers of the sample. Typical effusion profiles in Figs. 95.55 and 95.56 clearly show the presence of several peaks that are suggestive of different hydrogen–silicon binding states.

Infrared Spectroscopy

To investigate the bonding of tritium in the amorphous silicon network, we compared the infrared spectra of a hydrogenated (a-Si:H), a deuterated (a-Si:H:D), and a tritiated (a-Si:H:T) film of similar thickness (0.2 to 0.3 μm). Figure 95.57 shows the high-frequency part of the spectra for the three films, with the individual curves shifted vertically with respect to each other by approximately 500 cm^{-1}, for clarity. The vibrations near 2000 cm^{-1} in the a-Si:H film indicates Si–H stretching modes.[10] Very similar hydrogen peaks are observed in the a-Si:H:D and a-Si:H:T films grown with hydrogen originating from the silane gas. The deuterated and tritiated spectra show additional peaks near 1500 cm^{-1} and 1200 cm^{-1}, respectively. These peaks are attributed to Si–D

E12116

Figure 95.57
High-frequency IR vibrations of hydrogenated (H1), deuterated (D1), and tritiated (A214) amorphous silicon films. H1 and D1 have been offset with respect to A214 for clarity.

and Si–T stretching vibrations. The greater-reduced mass of the Si–D and Si–T oscillators relative to that of the Si–H oscillator is responsible for the shift to lower frequencies.

Using the harmonic potential approximation, the stretching frequencies of the Si–D(T) bonds can be calculated with respect to the Si–H bond-stretching frequency, i.e.,

$$\frac{\omega_{Si-D(T)}}{\omega_{Si-H}} = \sqrt{\frac{m_H\left[m_{D(T)} + M_{Si}\right]}{m_{D(T)}\left(m_H + M_{Si}\right)}}, \quad (2)$$

where $\omega_{Si-H(D,T)}$ is the stretching frequency of the Si–H(D,T) bond, $m_{H(D,T)}$ denotes the mass of hydrogen (deuterium, tritium), and M_{Si} represents the mass of silicon. Table 95.IV tabulates the experimental and calculated ratios.

Table 95.IV: Ratio of stretching frequency of Si–D and Si–T bonds with respect to Si–H bonds.

Ratio of Frequencies	Experimental	Calculated
$\omega_{Si-D}/\omega_{Si-H}$	0.73	0.72
$\omega_{Si-T}/\omega_{Si-H}$	0.61	0.60

The weak integrated intensity of the deuterium- and tritium-related vibrations, relative to that of hydrogen absorption bands, is expected since integrated intensity is inversely proportional to the reduced mass of the oscillator. An analysis of the lower-frequency modes (wagging, bending, etc.) leads to similar agreement between experimental and calculated values.[11] This shows that both deuterium and tritium behave as heavy hydrogen atoms in the amorphous silicon network and establish a similar bonding pattern.

Dangling Bonds in a-Si:H:T

When beta decay of tritium in a-Si:H:T occurs, a high-energy electron is released and the tritium nucleus transmutates into helium. The following processes take place in the material:

1. The beta particles created in the process of radioactive decay interact with the amorphous network and generate over 1000 electron-hole (e-h) pairs each.[12] The energy of the beta particle is insufficient, however, to cause irreversible lattice damage.[13,14]

2. The recoil energy of the helium is about 3 eV, which is insufficient to cause irreversible lattice damage.[14,15]
3. Helium does not stably bond with silicon; therefore, a silicon dangling bond is created at the site of each decayed tritium atom.

The rate of dangling-bond formation due to bonded tritium decay is

$$\frac{dN_{db}(t)}{dt} = \lambda N_T \exp(-\lambda t), \tag{3}$$

where N_{db} is the concentration of dangling bonds, N_T is the tritium concentration at $t = 0$, and λ is the decay rate of tritium.

Initially, the dangling bonds must be positively charged (D^+ centers); however, with time, the D^+ centers are expected to attract electrons and be converted into neutral dangling bonds (D^0 centers). This process should have a high probability due to the large number of free electrons present in the material. To stabilize the transition from a D^+ to D^0 center, however, a 15° bond-angle change is necessary.[16] This reduces the probability of the conversion; consequently, we expect that reemission of electrons will compete with the D^+ to D^0 conversion process and a steady concentration of D^+ and D^0 centers will develop, determined by the tritium decay and the electron reemission process.

We investigate the formation of dangling bonds using electron spin resonance and photoluminescence. The following two sections describe the approach and summarize the results.

Electron Spin Resonance

Electron spin resonance (ESR) provides a direct measurement of the concentration of Si-dangling-bond D^0 neutral defect states.[17] We have monitored concentrations of defects and studied their time evolution and annealing behavior in sample G181 (~0.6 μm thick) using a Bruker ESR spectrometer. Just after deposition, the tritium and hydrogen concentrations were 9 at. % and 22 at. %, respectively. The spin resonance was first measured after four years of storage. Due to the ongoing decay of tritium to helium, we expect the Si-dangling-bond defect concentration to be as high as $N_{db} = 5 \times 10^{21}$ cm^{-3} at the time of the ESR measurement. An additional degradation effect by emitted beta particles, if any, would make this concentration even higher. Surprisingly, however, the measured defect spin density was only $N_d = 6.4 \times 10^{17}$ cm^{-3}. Such a large discrepancy suggests that there is an ongoing process that either eliminates the created defects or

makes them invisible to ESR. The latter implies the creation of large numbers of charged defects. Dopant-like states capable of providing the necessary charge, however, are unlikely created by tritium decay. In addition, the created defects are not stable: they anneal out by heating at 150°C. This strongly suggests that their creation is likely counterweighted by an annealing process that takes place even at room temperature. As a result, defect density finally saturates at concentrations much lower than those of the decayed tritium atoms. This annealing is somewhat similar to the thermal decay of the Si-dangling-bond defects created by light (Staebler–Wronski effect[18]). In the latter case, typical annealing temperatures are above 150°C, while some of the defects do anneal even at room temperature due to their very broad spectrum of annealing activation energies.[19,20] The experimental evidence for the thermal annealing of defects in tritiated a-Si is outlined below.

After the ESR measurement, the four-year-old a-Si:H:T sample was annealed at 150°C for 30 min and then rapidly cooled down to room temperature; the evolution of the ESR signal with time was subsequently monitored. The results are shown in Fig. 95.58. Annealing reduced the spin concentration to 5.6×10^{16} cm^{-3}. After the annealing, the spin density increased rapidly, with an initial rate of creation of defect spins roughly equal to the rate of tritium decay (dashed line). After about 20 h, however, the rate of creation of spin states slowed down considerably, and the spin density again saturated at the old value of about 6.9×10^{17} cm^{-3} within one month. We have fitted this time evolution N_d by a stretched exponential dependence:

$$N_d(t) = N_0 + (N_{sat} - N_0) \times \left\{ 1 - \exp\left[\left(-\frac{t}{\tau}\right)^\alpha \right] \right\}, \tag{4}$$

where N_0 is the dangling-bond density at $t = 0$. The saturation value N_{sat} is approximately equal to the concentration of spin states measured after four years of storage, prior to annealing. Such dependence generally describes relaxation phenomena with time-dependent transition rates in disordered systems, including hydrogenated amorphous silicon.[3,16,21,22] The time constant τ of Eq. (4) approximately characterizes the lifetime of newly created defects and is about 12 days at room temperature. The thermal character of the defect equilibration was further confirmed by keeping the sample at an elevated temperature of 80°C after annealing. In this case, the defect concentration saturated in less than one day and the saturation value was below 10^{17} cm^{-3}. Such an effective annealing may be a result of very high concentrations of hydrogen and tritium

in our sample, leading to clustered hydrogen regions. Experiments on samples with lower H content are being planned. It is also a challenge to explain the annealing mechanism for the defects since the concentrations of the decayed tritium atoms after four years of sample storage are very high—of the order 10^{21} cm^{-3}. One might assume that H atoms that diffuse from nearby sites annihilate these defects. In this case, H detachment from such a site should not be accompanied by the creation of a new defect. This might be possible if H comes from a large reservoir of paired H sites such as double-hydrogen complexes[23] or hydrogenated vacancies.[24] Further experiments are necessary to elucidate the mechanism of defect annealing.
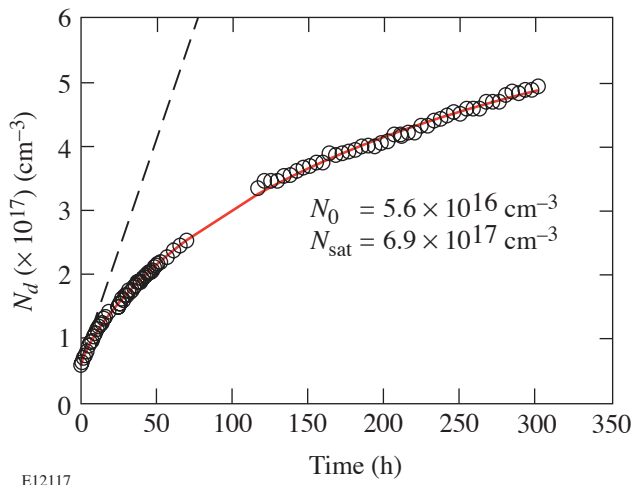
E12117

Figure 95.58
ESR results for sample G181 after 30 min annealing at 150°C. The solid curve is a fit to the data using Eq. (4). The values of the parameters obtained from the fit are indicated in the figure. The dashed line represents the number of tritium decays calculated using Eq. (3).

Photoluminescence

Photoluminescence (PL) of the films was measured using an Ar$^+$ ion laser tuned to 490 nm. Shortly after deposition, the tritiated samples exhibited strong, low-temperature PL. The PL spectrum at 5 h after deposition and its temperature dependence were similar to those observed in samples deposited under similar conditions except for hydrogen or deuterium in place of tritium in the feed gas stream. This confirms that the density-of-states (DOS) distribution in the films does not depend strongly on the hydrogen isotope used in the feed gas stream. However, the PL of the tritiated samples decreases quickly with time, due to the creation of dangling bonds that act as recombination centers for the electron-hole (e-h) pairs, thus quenching the luminescence signal.[16]

In Fig. 95.59 the decay of the photoluminescence is plotted as a function of time for the three successive annealing cycles of sample A206 (~0.2 μm thick). We annealed the samples at 150°C for 30 min for each cycle. The data for the initial photoluminescence decay, immediately following deposition, for sample A170 (~0.6 μm thick) are also included in the figure. It is seen to be similar to the data for sample A206. Neutral dangling bonds (D^0) are the most-effective recombination centers for e-h pairs[16] and are therefore the most likely cause of the quenching of the PL signal. The solid line in Fig. 95.59 is based on the theoretical model of Sidhu et al.[25] and the values of N_d obtained from ESR measurements. According to Sidhu's model, the PL efficiency η can be written as

$$\eta = \frac{1}{1 + \tau v \exp\left[-\frac{2}{R}\left(\frac{4\pi}{3}N_d\right)^{-1/3}\right]}, \tag{5}$$

where v is the attempt to hop frequency, τ is the radiative lifetime, and R is the tunneling radius. Table 95.V presents the values of the parameters obtained from the fit and the expected range for these parameters.

It should be noted that in an earlier paper[25] we attributed the decrease in the PL signal entirely to primary dangling bonds created through tritium decay. Over 50% of the PL decrease occurs during the first 30 h after annealing, where $D^+ \approx D^0$. Later D^+ and D^0 diverge; however, the difference in the predicted PL signal is relatively small since the concentration of dangling bonds is quite high after the first 30 h.
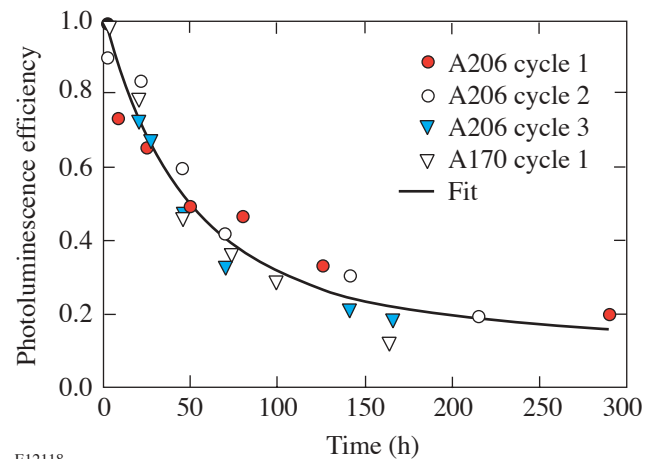
E12118

Figure 95.59
PL efficiency versus time for samples A206 (three cycles) and A170 (one cycle). The points represent the area of the normalized PL signals. The solid line was obtained from the model developed by Sidhu et al.[25]

Table 95.V: Measured and expected values for the parameters in Eq. (5). The column labeled "fitted value" uses Eq. (4) in the Sidhu model. The "expected range" values are from the literature.

Parameter	Fitted Value	Expected Range[3,4,26–28]
R	2.9 nm	1.3 to 10 nm
$\nu\tau$	1150	$N \sim 10^{11-13}$ s^{-1}, $t \sim 10^{-8,-9}$ s

Betavoltaics

Our intrinsic betavoltaic device consists of a tritiated amorphous semiconductor p-i-n junction. The beta-induced electron-hole pairs are separated by the electric field present in the depletion region of the junction. This is similar to conventional betavoltaic or photovoltaic cells except that it is powered by intrinsic tritium decay betas rather than external electrons or external photons, respectively. A schematic illustrating the intrinsic betavoltaic device is shown in Fig. 95.60.

The maximum power density P_{max} for this configuration was measured to be $P_{max} = 0.29$ μW/cm^2 (per 48 mCi/cm^2 per μm at 20 at. % tritium), which is approximately 16% of the theoretical maximum attainable power.[29] Alternatively, stacking a number of such cells in series and/or in parallel would require approximately 330 Ci to achieve a 1-mW tritium powered battery. A 1-mW battery is defined as that having this power output at the end of one tritium half-life, i.e., approxi-
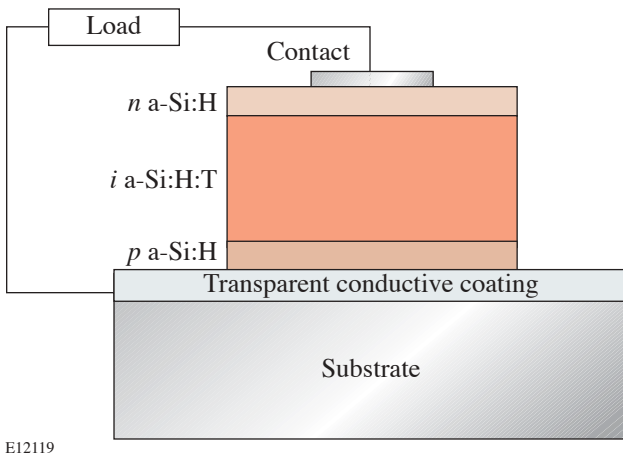
mately 12 years; tacit in this definition is that the cell power output diminishes at a rate equal to the decay of tritium atoms.

As described in the previous sections, however, tritium decay creates dangling bonds. When the density of dangling bonds increases, a nonuniform electric field develops in the intrinsic region of the p-i-n junction and the effective width of the space charge region is reduced.[30] The reduced electric field near the middle of the intrinsic region reduces the velocity of carriers and thereby increases the probability of electron-hole-pair recombination. This in turn reduces the number of electron-hole pairs available for electrical power, and the output power from the betavoltaic device decreases.

As discussed earlier, dangling bonds are inevitably created as a consequence of the radioactive decay of the bonded tritium. Fortunately, the effect of these dangling bonds on the betavoltaic device can be reduced by confining the tritium to small regions of the otherwise hydrogenated amorphous silicon intrinsic region. We used a thin slice of tritiated material and refer to this as a *delta* layer configuration. Now, rather than the entire intrinsic region being comprised of dangling bonds, only a fraction of it will contain a large concentration of dangling bonds. As a result, a uniform electric field will exist across most of the intrinsic region, and degradation of the betavoltaic device will be limited.

A p-i-n *delta* layer device is illustrated in Fig. 95.61. The p and n layers of the p-i-n delta layer devices were deposited

E12119

Figure 95.60
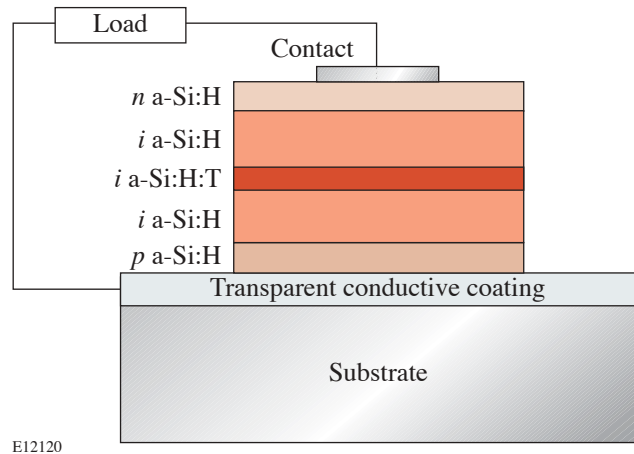Schematic design of an intrinsic betavoltaic device.

E12120

Figure 95.61
Schematic design of a *p-i-n delta* layer device.

using a 2% gas mixture of B_2H_6 in SiH_4 and PH_3 in SiH_4, respectively. The thickness of the *p* layer was approximately 120 Å, while the thickness of the *n* layer was approximately 200 Å. The hydrogenated portions of the intrinsic region for the devices were grown using undiluted SiH_4, and the thickness was approximately 0.12 μm. The tritiated delta layer was deposited using tritium gas and SiH_4. These gasses were introduced into the plasma at equal gas-flow rates of 4 standard cc/min (sccm). The deposition time was used to control the thickness of the delta region. The total chamber pressure was maintained at 140 mTorr for the time required to grow the entire intrinsic region. While growing all layers, the substrate temperature was 250°C. The anode voltage during deposition of the layers was approximately 620 V while the anode current was approximately 12 mA.

The behavior of devices with a delta layer was compared with a device whose entire intrinsic region was tritiated. We label this last device *uniform* while the three devices with a delta layer were labeled *delta* 1, 2, and 3. The thickness of the tritiated layer in *delta* 1 was approximately 1/3 the thickness of the intrinsic layer in the device *uniform*. Similarly, the thickness of the a-Si:H:T layer in *delta* 2 and *delta* 3 were approximately 1/6 and 1/12 the thickness of the intrinsic layer in the device *uniform*, respectively. The concentration of tritium in the tritiated region of all devices was similar at about 5 at. %. Table 95.VI gives the short-circuit current and open-circuit voltage for the four devices, measured shortly after their manufacture.

structure of the delta devices is similar, the open-circuit voltages decrease monotonically with the short-circuit current. The open-circuit voltage of *delta* 3 did not decrease in comparison to *delta* 2. This is most likely the result of a better junction in *delta* 3. The smaller-than-expected short-circuit current from *delta* 3 is most likely due to a thinner-than-expected delta layer; the very short deposition time makes it difficult to accurately deposit the delta layer, which was expected to be 300 μm thick.

For each device, the short-circuit current under dark conditions was measured as a function of time. The remaining fraction of the initial short-circuit current as a function of time is plotted in Fig. 95.62. After approximately 200 h, the short-circuit current for *uniform* was less than 10% of its initial value. The decrease in the fractional short-circuit current for the delta-layered devices was not as rapid, and, as can be seen in Fig. 95.62, the short-circuit currents appeared to settle asymptotically to a fractional value greater than that of *uniform*. The short-circuit current for *delta* 3 decreased by only approximately 50% from its initial value after 600 h of operation. This difference in behavior is because dangling bonds in the *delta* devices are isolated within a small, tritiated portion of the intrinsic region. Initially, in all the devices, there would have been a uniform electric field across the intrinsic region; however, as dangling bonds are created, the electric field weakens in a-Si:H:T sections. In the device *uniform*, the electric field is weakened throughout most of the intrinsic region. In the *delta* devices, a weak electric field exists only in the delta layer. To

Table 95.VI: Short-circuit current and open-circuit voltage for the *delta* devices and the device *uniform*.

Device	I_{sc} (nA)±2%	V_{oc} (mV)±0.2%
uniform	0.98	21
delta 1	0.35	20
delta 2	0.14	9
delta 3	0.03	11

Of the four devices listed in Table 95.VI, the device *uniform* has the largest short-circuit current. On the whole, the differences in the short-circuit current among the devices are consistent with the difference in the thickness of the tritiated amorphous silicon layer. As the thickness of the tritiated layer is reduced, fewer beta particles are created; hence, the number of electron-hole pairs created is reduced by nearly the same ratio. Since the
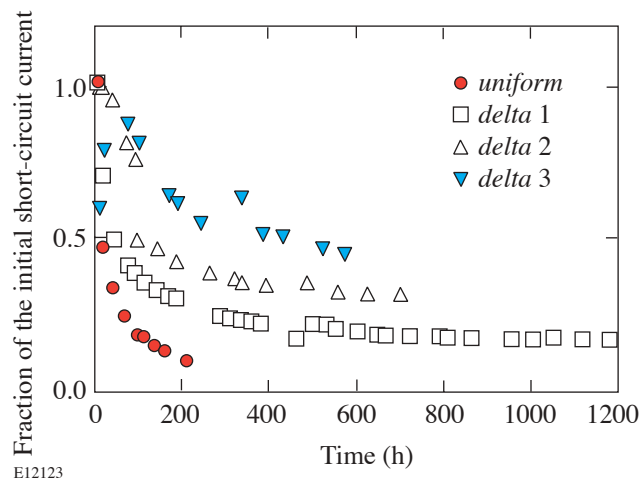

E12123

Figure 95.62
Short-circuit current as a function of time in the *p-i-n* devices.

accommodate the reduced electric field in the a-Si:H:T delta layer, the electric field strengthens in the a-Si:H region, increasing the drift velocity of carriers and helping carriers traverse the intrinsic region without recombination. This increased drift velocity in the untritiated region will have little effect, however, on the short-circuit current once the thickness of the tritiated region exceeds the diffusion length of the carriers.

A numerical simulation was carried out to determine the spatial distribution of the beta-particle energy deposited in the intrinsic regions as a function of the delta-layer thickness and the resulting initial short-circuit current.[31] The results of the simulations are summarized in Table 95.VII. It can be seen that as the thickness of the a-Si:H:T region is reduced, increasingly more energy is deposited in the a-Si:H regions rather than in the a-Si:H:T region. This is to be expected since as the *delta* layer becomes thinner, relatively fewer electron-hole pairs are created in the a-Si:H:T region than in the a-Si:H region since less energy is deposited in the a-Si:H:T than in the a-Si:H region.

The energy transferred from a beta particle to the amorphous silicon lattice is given by the stopping power of the material as the particle moves through the material. There is a broad distribution of kinetic energies of the beta particles from the decay of tritium (Fig. 95.52). The initial kinetic energy of the beta particle can be averaged between the most-probable energy of about 3 keV and the average energy of 5.7 keV. The energy deposited in each section of the intrinsic region was simulated using a uniform distribution of bonded tritium atoms and taking into account the path length traveled by the beta particle as it loses energy to the lattice. The results of this calculation together with the corresponding experimental results are presented in Table 95.VIII. It can be seen that the numerical calculations agree quite well with the experimental data.

Conclusions

Tritium bonds stably in amorphous silicon. This is confirmed by outgassing, effusion, and infrared spectroscopy. The radioactive decay of tritium gives rise to the formation of dangling bonds as a consequence of tritium transmutation into helium; however, the number of dangling bonds appears to be much less than the number of decayed tritium atoms, most likely due to some form of lattice reconstruction.

Electron-hole pairs created by beta particles emitted in the process of tritium decay are separated by the built-in field of a tritiated amorphous silicon *p-i-n* junction. Dangling bonds formed in the process of tritium decay cause degradation of the current–voltage characteristic of the *p-i-n* junction with time.

Table 95.VII: Distribution of the beta-particle energy.

Device	a-Si:H (top/bottom layer) (%)				a-Si:H:T (*delta* layer) (%)			
	Energy (keV)				Energy (keV)			
	1	2	3	5.7	1	2	3	5.7
delta 1	6.9	20	35	34	87	60	30	31
delta 2	13.7	36	43	40	36	27.4	15	19
delta 3	27.3	43.5	46	45	22.7	13	8.3	11

Table 95.VIII: Asymptotic value of the short-circuit current as a fraction of the initial short-circuit current for the three *delta* devices.[31]

Device	Experiment	Numerical
delta 1	0.15	0.27
delta 2	0.30	0.36
delta 3	0.45	0.42

This degradation can be controlled, however, by confining the tritium to small volumes in the *p-i-n* junction. Consequently, tritiated amorphous silicon may find an application in self-powered *p-i-n* junction betavoltaic batteries.

REFERENCES

1. R. A. Street, *Technology and Applications of Amorphous Silicon*, Springer Series in Materials Science, Vol. 37 (Springer, New York, 2000).

2. G. Bruno, P. Capezzuto, and A. Madan, eds. *Plasma Deposition of Amorphous Silicon-Based Materials*, Plasma–Materials Interactions (Academic Press, Boston, 1995).

3. R. A. Street, *Hydrogenated Amorphous Silicon* (Cambridge University Press, Cambridge, England, 1991), p. 203.

4. W. Fuhs, in *Amorphous and Microcrystalline Semiconductor Devices*, edited by J. Kanicki (Artech House, Boston, 1992), Chap. 1, Vol. II, pp. 1–53.

5. W. Luft and Y. S. Tsuo, *Hydrogenated Amorphous Silicon Alloy Deposition Processes*, Applied Physics, Vol. 1 (Marcel Dekker, New York, 1993).

6. G. Vasaru, *Tritium Isotope Separation* (CRC Press, Boca Raton, FL, 1993).

7. N. P. Kherani, "Electron Flux and Energy Distribution at the Surface of Lithium Tritide," Ph.D. thesis, University of Toronto, 1994.

8. N. P. Kherani, K. Virk, T. Kosteki, F. Gaspari, W. T. Shmayda, and S. Zukotynski, "Hydrogen Effusion from Tritiated Amorphous Silicon," to be published in *IEE Proceedings Circuits, Devices and Systems Special Issue on Amorphous and Microcrystalline Semiconductor Devices*.

9. W. T. Shmayda, A. B. Antoniazzi, and R. A. Surette, Ontario Hydro Research Division, Toronto, Canada, report no. 92-51-K (1992).

10. M. Stutzmann, in *Properties of Amorphous Silicon and Its Alloys*, edited by T. Searle (INSPEC, IEE, London, 1998), pp. 56–60.

11. L. S. Sidhu *et al.*, J. Appl. Phys. **85**, 2574 (1999).

12. T. Kosteski, N. P. Kherani, F. Gaspari, S. Zukotynski, and W. T. Shmayda, J. Vac. Sci. Technol. A **16**, 893 (1998).

13. U. Schneider, B. Schroder, and F. Finger, J. Non-Cryst. Solids **114**, 633 (1989).

14. M. Stutzmann, in *Amorphous and Microcrystalline Semiconductor Devices*, edited by J. Kanicki (Artech House, Boston, 1992), Chap. 4, Vol. II, pp. 129–187.

15. R. Street, D. Biegelsen, and J. Stuke, Philos. Mag. B **40**, 451 (1979).

16. R. S. Crandall, Phys. Rev. B, Condens. Matter **43**, 4057 (1991).

17. P. C. Taylor, in *Properties of Amorphous Silicon and Its Alloys*, edited by T. Searle (INSPEC, IEE, London, 1998), Sec. 3.3, pp. 139–142.

18. D. L. Staebler and C. R. Wronski, Appl. Phys. Lett. **31**, 292 (1977).

19. P. Stradins and H. Fritzsche, Philos. Mag. B **69**, 121 (1994).

20. Q. Zhang *et al.*, in *Symposium on Amorphous Silicon Technology – 1994*, edited by E. A. Schiff *et al.* (Materials Research Society, Pittsburgh, PA, 1994), pp. 269–274.

21. A. Tagliaferro, Mod. Phys. Lett. B **4**, 1415 (1990).

22. J. Kakalios, R. A. Street, and W. B. Jackson, Phys. Rev. Lett. **59**, 1037 (1987).

23. H. M. Branz, Phys. Rev. B, Condens. Matter **59**, 5498 (1999).

24. S. B. Zhang and H. M. Branz, Phys. Rev. Lett. **87**, 105503 (2001).

25. L. S. Sidhu, T. Kosteski, S. Zukotynski, N. P. Kherani, and W. T. Shmayda, Appl. Phys. Lett. **74**, 3975 (1999).

26. R. A. Street and D. K. Biegelsen, in *Physics of Hydrogenated Amorphous Silicon II. Electronic and Vibrational Properties*, edited by J. D. Joannopoulos and G. Lucovsky (Springer-Verlag, Berlin, 1984), pp. 195–259.

27. W. C. Chen and L.-A. Hamel, in *Symposium on Amorphous Silicon Technology – 1996*, edited by M. Hack *et al.* (Materials Research Society, Pittsburgh, PA, 1996), pp. 759–764.

28. B. A. Wilson *et al.*, Phys. Rev. Lett. **50**, 1490 (1983).

29. N. P. Kherani, T. Kosteski, S. Zukotynski, and W. T. Shmayda, Fusion Technol. **28**, 1609 (1995).

30. K. R. Lord, II, M. R. Walters, and J. R. Woodyard, in *Proceedings of the XIII Space Photovoltaic Research and Technology Conference*, NASA Conference Publication 3278 (NASA Lewis Research Center, Washington, DC, 1994), pp. 187–196.

31. T. Kosteski, "Tritiated Amorphous Silicon Films and Devices," Ph.D. thesis, University of Toronto, 2001.